Indian Summer Monsoon Simulations In Successive Generations Of The NCAR Community Atmosphere Model

Ravi Kumar
Indian Institute of Technology Delhi
Raju Pathak (rajuphyamu@gmail.com)
Indian Institute of Technology Delhi
Sandeep Sahany
Indian Institute of Technology Delhi
Saroj K. Mishra
Indian Institute of Technology Delhi

Research Article

Keywords: Climate Modeling, NCAR CAM, Indian Summer Monsoon, MISO

Posted Date: May 4th, 2021

DOI: https://doi.org/10.21203/rs.3.rs-418615/v1

Version of Record: A version of this preprint was published at Theoretical and Applied Climatology on June 12th, 2023. See the published version at https://doi.org/10.1007/s00704-023-04514-0.

Abstract

Four generations of the NCAR Community Atmosphere Model (CAM-3, 4, 5, and 6) are evaluated for the Indian summer monsoon (ISM) simulations. Total precipitation simulated by successive versions of CAM is overestimated over the western equatorial Indian Ocean (EIO), Arabian Sea, and Western Ghats (WGs), and underestimated over the eastern EIO, Bay of Bengal (BoB), and Indo-Burmese mountains, due to overestimated convective and underestimated large-scale precipitation, respectively. Overestimation of total precipitation over the Himalayan region is increased in successive CAM variants, primarily through enhanced large-scale precipitation. Improvement in total precipitation simulation over BoB is found in successive CAM variants, with the largest improvement in CAM6. The frequency of total precipitation is overestimated for low precipitation rates and underestimated for high precipitation rates in CAM variants, except in CAM4 for high precipitation rates.

The subtropical westerly and tropical easterly jets are better simulated in CAM5-6 than CAM3-4 (highly overestimated). The easterly shear of zonal wind during the peak monsoon is highly overestimated in all CAM variants. The monsoon low-level jet over AS and peninsular India is overestimated in all CAM variants with the largest overestimation in CAM6, resulting in increased precipitation over WGs and peninsular India. We find the large underestimation in a tropical easterly jet over peninsular India and EIO in CAM3 to have improved in the successive versions. In addition, overestimation of the strength of the subtropical westerly jet and the Tibetan anticyclone seen in CAM3 has improved in successive variants of CAM. We find improvements in monsoon intra-seasonal oscillation (MISO) and associated internal dynamics and the east-west and north-south heat source in successive variants of CAM. Overall, we find many improvements in the simulation of ISM precipitation and its associated dynamics in successive variants of CAM, however, there still remain some important biases (e.g., eastward component of MISO, monsoon low-level jet, excessive precipitation over Himalayan foothills, early monsoon onset, etc.) that need to be alleviated for more realistic ISM simulations in future versions of CAM.

Introduction

Reliable simulations of spatio-temporal variability of the Indian summer monsoon (ISM) is crucial for the socio-economic well-being of one-sixth of the world population residing in India (e.g., Parthasarathy et al. 1988; Kumar et al. 2004; Gadgil and Gadgil 2006; Dunning et al. 2015). The ISM rainfall (June to September; JJAS) contributes ~ 70–80% to the annual rainfall (e.g., Webster et al. 1998; Goswami 1998; Rajeevan et al. 2012; Sahany et al. 2018). Its simulation has been challenging to the numerical modeling community (e.g., Covey et al. 2003; Trenberth et al. 2003; Sperber et al. 2013). For example, Gadgil and Sajani (1998) reported problems simulating observed monsoon variability and the seasonal mean rainfall pattern for most of the climate models in one of the early Atmospheric Model Intercomparison Project (AMIP) set of simulations. Sperber and Palmer (1996) have noted that models that simulate rainfall climatology well also simulate improved inter-annual variability. Sperber et al. (2013) have reported that no single model in Coupled Model Intercomparison Project phase-3 (CMIP3) or phase-5 (CMIP5) can better simulate the annual cycle, inter-annual, and intra-seasonal variability of ISM rainfall. However, he

also noted that CMIP5 is much better than CMIP3 in representing ISM's different aspects. Pathak et al. (2019) identified systematic biases in the seasonal mean monsoon precipitation for many of the CMIP5 and AMIP5 models and noted a common bias in simulating convective and large-scale precipitation across the models. He also indicated that the closure and trigger assumptions used in the convection parameterization schemes are primarily responsible for these biases. Some other studies have noted that the ISM biases in GCMs could be arising from the cold sea surface temperature (SST) biases over the northern Arabian Sea (AS), improper representation of sub-grid processes, resolution-independent parameterizations, coarse topography, incorrect initial and boundary conditions, and improper coupling of model components (e.g., Bollasina et al. 2009; Sukumaran et al. 2014; Ramu et al. 2016; Koul et al. 2018; Pathak et al. 2019, 2020).

In addition to the ISM rainfall, reliable simulations of associated dynamical features, such as the low-level jet, Tibetan anticyclone, tropical easterly and subtropical westerly jets, Intertropical convergence zone, and the regional Hadley and planetary-scale Walker circulation are also crucial for monsoon studies (e.g., Rao 1976, Sikka 1980, Gadgil 2003, Krishnamurthy and Kinter 2003, Annamalai et al. 2007, Lau et al. 2015, Fan et al. 2017). However, simulations of the aforementioned dynamical features are also biased in existing GCMs. For example, the mean Walker circulation is underestimated in many GCMs, due to the low SST gradient in the zonal direction (Zhou and Xie 2014). The low-level jet (Somali jet) is simulated unsatisfactorily due to a large bias in convective heating over peninsular India and the equatorial Indian Ocean (EIO) (Attada et al. 2014). Such biases lead to unrealistic simulations of the ISM intra-seasonal variability and strength (Joseph et al. 2012; Sharmila et al. 2012; Sperber et al. 2013). In general, biases in the zonal wind's vertical shear affect the northward moisture transport from the ocean to the Indian subcontinent by changing the atmospheric instability and associated convective activity (Zhou and Murtugudde 2014). This further affects the active and break spells, and hence the simulation of precipitation variability on the intra-seasonal time scale (e.g., Sikka and Gadgil 1980; Goswami 2011).

While there are biases in most of the latest generation climate models in simulating the ISM, the National Center for Atmospheric Research (NCAR) Community Earth System Model (CESM) is one of the better performing models (e.g., Douville et al. 2000; Knuti et al. 2013; Pascale et al. 2014; Anand et al. 2018; Pathak et al. 2020). In the last couple decades, there have been major changes in the physics and dynamics of the NCAR climate model, as it evolved from CCSM3 (CAM3 atmospheric component) through CESM2 (CAM6 atmospheric component). Specifically, in CAM4, the deep convection scheme of CAM3 was modified to include dilute parcel entrainment (Neale et al. 2008) and convective momentum transport (Richter and Rasch 2008). The cloud fraction scheme of CAM3 was modified to account for the cloud fraction thermodynamically consistent with the condensate value (Vavrus and Waliser 2008) and the radiation scheme was also slightly updated (Gent et al. 2009). In CAM5, the turbulence scheme was replaced by a new moist turbulence scheme based on diagnostic turbulent kinetic energy (Park et al. 2009), and the cloud microphysics scheme was modified to have a more optically transparent occurrence of cloud processes and consistency between cloud fraction and cloud condensate (Park et al. 2010). In CAM6, the shallow convection, cloud macrophysics, and boundary layer turbulence scheme was combined to a single Cloud Layers Unified by Binormals (CLUBB) scheme (Golaz and Larson 2002;

Bogenschutz et al. 2013), the cloud microphysics scheme was updated using Gettelman and Morrison (2015), and the aerosol scheme was revised to 4-Mode Modal aerosol scheme.

The above mentioned improvements in the physics package of the successive versions of the NCAR CAM have motivated us to assess their impact on ISM simulation in CAM3, 4, 5, and 6. Our study will investigate how these model upgrades have impacted ISM simulation. We provide an introduction in Sect. 1 and data and methodology in Sect. 2. We present the result and discussion in Sect. 3. In particular, we show the seasonal mean ISM pattern in Sect. 3.1, horizontal wind pattern in Sect. 3.2, tropospheric temperature gradient and easterly wind shear in Sect. 3.3, and the monsoon intra-seasonal oscillation in Sect. 3.4. Section 3.4 further presents the regional Hadley and planetary-scale Walker circulation in Sect. 3.4.1 and atmospheric internal dynamics in Sect. 3.4.2. Section 4 concludes the study with the results, findings, and future scope.

Data, Model, And Simulation Details

2.1 Data

We have used satellite-derived monthly total, convective, and large-scale precipitation from Tropical Rainfall Measuring Mission (TRMM) 3A12 for 2000–2015 and daily total precipitation from TRMM 3B42 for 2000–2015 (Huffman et al. 2007). The horizontal and vertical wind, temperature, and specific humidity are used from the European Centre for Medium-Range Weather Forecasts Interim reanalysis (ERA-I) for 2000–2015 (Dee et al. 2011). The observed and reanalysis datasets are interpolated to model resolution.

2.2 Model and Simulation Details

Successive versions of the NCAR CAM (namely, 3, 4, 5, and 6; see Collins et al. 2004; Neale et al. 2010, 2012; Danabasoglu et al. 2020) were forced with prescribed monthly varying climatological (1982–2002) SSTs (Reynolds et al. 2002). The monthly values are linearly interpolated in time to prescribe daily varying SSTs in the model. More details on CAM configurations can be found in Table 1. The horizontal resolution used in model simulations for all CAM variants is 0.9° latitude and 1.25° longitude). The number of vertical levels used in model simulations is the default setup, i.e., for CAM3-4, it is 26 levels, for CAM5, it is 30 levels, and for CAM6, it is 32 levels. Using the above setups, we performed 15 years of simulation for each CAM variant.

Results And Discussion

3.1 Mean Pattern of Indian Summer Monsoon

Figure 1 compares the model simulated seasonal mean total, convective, and large-scale precipitation with corresponding observations. For total precipitation, observation shows the highest values (> 8 mm/day) over the north-eastern Bay of Bengal (BoB), Indo-Burmese mountains, foot-hills of Himalaya, and Western Ghats (WGs); moderate values (> 3 mm/day and < 8 mm/day) over the eastern EIO, central

India, and eastern AS; and lowest values (< 3 mm/day) over the western AS, northwest India, leeward side of WGs, and western EIO (Fig. 1a). From the difference plot for total precipitation, it is noted that CAM3 simulates quite well over WGs and central India. However, there is a large wet bias over the western EIO and south-eastern coastal India and dry bias over the north-eastern BoB and Indo-Burmese mountains (Fig. 1b). While these wet and dry biases were alleviated significantly in CAM4, a new significant wet bias emerged over WGs, eastern AS, and the Himalayan region (Fig. 1c). In CAM5, the wet bias over eastern AS and WGs was alleviated to a large extent. The existing wet bias over the Himalayan region and dry bias over the north-eastern BoB was increased (Fig 1d). In CAM6, many of the existing wet and dry biases are reduced; however, the wet bias over WGs and the Himalayan region remains, and the wet bias over peninsular India has worsened (Fig. 1e).

Further splitting total precipitation into convective and large-scale components, we find that the observed spatial pattern of both components is similar to total precipitation except lesser in magnitude (Fig. 1f,k). It is also noted that both convective and large-scale components contribute nearly equally to the total precipitation over the ISM region. The difference plot for convective precipitation shows that CAM3 has a large wet bias over the south-eastern coast of India and western EIO (Fig. 1g). The wet bias over western EIO and south-eastern coast of India is greatly reduced in CAM4, but the wet bias over the Himalayan region and eastern AS is substantially increased (Fig. 1h). In CAM5, the existing wet biases are further reduced, except the wet bias over the Himalayan region, which is slightly increased (Fig. 1i). Compared to its predecessors, CAM6 shows a notable improvement in existing biases for convective precipitation (Fig. 1j). Further, the difference plot for large-scale components shows the large dry bias in CAM variants over the north-eastern BoB and Indo-Burmese mountains (Fig. 1l). While this dry bias in CAM4 was reduced substantially, a new wet bias emerged over the Himalayan region (Fig. 1m). In CAM5, these existing wet and dry biases were increased (Fig. 1n). However, in CAM6, the existing dry biases were greatly reduced (Fig. 1o). Thus, the wet bias over the Himalayan foothills and dry bias over the north-eastern BoB in the successive CAM variants are arising primarily through the wet and dry biases in large-scale precipitation, respectively.

Furthermore, for the annual cycle of total precipitation (Fig. 2a), we find a large dry bias in CAM3 and wet bias in CAM4 during June to October (highest during the peak monsoon period). In the successive CAM variants (CAM5-6), this wet bias seen in CAM4 is reduced substantially, but in CAM6 during June-July, the wet bias is slightly worsened with respect to CAM5. Past research findings have suggested that the cold and warm SST biases over EIO in a model can cause the dry and wet bias over the Indian land region and hence leading to the dry and wet bias in the annual cycle, respectively (Roxy et al. 2012; Joseph et al. 2012). From the frequency-intensity distribution of daily total precipitation rates over India during JJAS (Fig. 2b), we find that all CAM variants overestimate the frequency of light precipitation rate (<10 mm/day) and underestimate the frequency of large to extreme precipitation rate. The underestimation in the frequency of large to extreme precipitation is largest in CAM3 (which does not report any event > 90 mm/day) and is reduced relatively in CAM4 and CAM5. While in CAM6, the underestimation in the frequency of extreme precipitation rate is increased compared to CAM4 and CAM5. Such overestimation in the frequency of light precipitation rates and underestimation in the frequency of extreme precipitation

rates have also been noticed in many of the CMIP5 models (e.g., Dai 2006; Deng et al. 2007; Mishra et al. 2018; Salunke et al. 2019).

3.2 Horizontal Wind Pattern

Figure 3 shows the seasonal mean pattern of atmospheric circulations at 850 hPa and 200 hPa from ERA-I and CAM variants. It is noted that CAM variants simulate the circulation patterns comparable to ERA-I, for example, the simulation of low-level cross-equatorial westerlies, low-level cyclonic wind over northern India, TEJ (with maximum intensity over peninsular India), subtropical westerly jet (STJ), and Tibetan anticyclone. However, from the difference plot at 850 hPa, we find that CAM3 underestimates the south-westerly wind over peninsular India and BoB, resulting in an underestimation of total precipitation over BoB and Indo-Burmese mountains due to reduced moisture transport (e.g., Swapna and Kumar 2002; Puranik et al. 2014). In CAM4, 5, and 6, we find an overestimation of the south-westerly wind over AS and peninsular India, with largest overestimation in CAM6, resulting in an increased precipitation over WGs and peninsular India (e.g., Swapna and Kumar 2002; Ratna et al. 2014).

From further analysis of the difference plot at 200 hPa, we find that CAM3 shows large underestimation in TEJ over peninsular India and EIO, which could be a reason for the weakened vertical easterly wind shear (see Section 3.3) and hence the weakening of the monsoon circulation and associated precipitation (Fig. 1). The association of the weakening (strengthening) of TEJ and decrease (increase) in tropical summer precipitation is also reported in past studies (e.g., Koteswaram 1958; Kanamitsu et al. 1972; Kobayashi 1974; Pielke et al. 2001; Sathiyamoorthy 2005; Sreekala et al. 2014). Furthermore, we find an overestimation in the core of STJ in CAM3. Modulations in the core of STJ have been reported to influence the precipitation distribution over northern India through modulation of the Tibetan anticyclone (Ramaswamy 1962). However, circulation biases seen in CAM3 have improved in the successive versions with advances in model physics.

3.3 Tropospheric Temperature Gradient and Easterly Wind Shear

Figure 4a depicts the tropospheric temperature gradient (ΔTT), computed as the difference in vertically (600-200 hPa) averaged temperature between the northern box (5°-35°N; 40°-100°E) and southern box (15°S-5°N; 40°-100°E). These two boxes represent the large-scale temperature gradient zones responsible for the seasonal reversal of winds over the ISM region due to the differential heating, primarily over the Tibetan plateau (Gill,1980; Yanai et al. 1973; Webster et al. 1998; Goswami and Xavier 2005; Xavier et al. 2007). Increased ΔTT suggests stronger monsoon circulation and increased associated precipitation. The onset and withdrawal are also established when ΔTT changes sign from negative to positive and from positive to negative, respectively. ERA-I shows monsoon onset in late May, peak precipitation in July and August, and withdrawal in early October, also noticed in other studies (Dey 1970; Indian Meteorological Department (IMD) 1972; Fasullo et al. 2003). Similar characteristics of ΔTT are noticed in CAM variants. However, the monsoon onset and withdrawal are simulated earlier than observed, by one to two weeks in CAM variants, except CAM6, which shows early onset but similar withdrawal as ERA-I (and

hence a prolonged monsoon season). ΔTT during JJAS is largely overestimated in CAM6, resulting in strengthening of low-level jet (Fig. 3) and an overestimation in precipitation over peninsular India (Fig. 1).

We also show the annual cycle of easterly wind shear (Fig. 4b), which is defined as the difference in the zonal wind between 850 hPa and 200 hPa, averaged over peninsular India (0 - 15°N; 50°-90°E) (Webster and Yang 1992; Jiang et al. 2004). This is known to cause vertically integrated moisture to propagate northward (EIO to central India), affecting atmospheric instability and convective activity over central India (Zhou and Murtugudde 2014). ERA-I shows a change from negative to positive wind shear in late April, with peaks in July and August, then positive shear until November (Fig. 4b). From our simulations, we found that CAM3 fails to accurately simulate this shear, although the subsequent CAM variants show improvements but still underestimate it, except CAM6. CAM6 simulates this shear close to ERA-I (compared to its predecessors), with slight overestimation in June to August, resulting in a better monsoon simulation and moisture transport towards BoB. This overestimated easterly wind shear in CAM6 (through enhanced low-level wind strength) could be a reason for an increase in precipitation over peninsular India (Fig. 1e).

3.4 Monsoon Intra-seasonal Oscillations (MISO)

One of the most significant modes of ISM variability is the 30-60 day oscillations of northward propagating convection anomalies over the ISM region (e.g., Goswami et al. 1998; Sharmila et al. 2012; Joseph et al. 2012). This northward propagating convection anomalies from EIO to the Indian subcontinent from June to September is referred to as the monsoon intra-seasonal oscillations (MISO). It is reported to explain more than 20% of the total JJAS rainfall variance over the Indo-Pacific region (Goswami et al. 1998). During the summer monsoon, the active and break spells have also been linked to MISO (e.g., Joseph et al. 2009; Krishnan et al. 2009; Goswami et al. 2011). In Figure 5, we show the space-time evolution of MISO from day -20 to +10 for observations and CAM variants. It is computed as a time-series of normalized area-averaged filtered (20-100 day) precipitation anomalies over central India (15°-25°N; 70°-90°E), with 20-100 day filtered precipitation anomalies regressed at different time lags during JJAS. The precipitation maximum over central India is thus on day 0 of MISO. From observations, the convection initiation occurs over central EIO on about day -20, and it spreads eastward (day -15) and then moves north-eastward to the Indian subcontinent by day -5. Around day 0, MISO has a strong eastward tilted convection band over the monsoon trough region and suppressed convection over EIO (Annamalai and Slingo 2001). This convection band shifts to Himalayan foothills by day +10, accompanied by corresponding north-eastward movement of the negative anomalies from EIO. Simulations show that CAM3 fails to capture the MISO pattern, but the successive CAM variants show the initiation of organized convection over central EIO and subsequent north-eastward movement comparable to observations. However, in CAM4, there is early suppression of convection (about -15 to -10 days) followed by enhanced convection (from day 0 onward) over EIO, but this is greatly improved in the subsequent variants, namely, CAM5 and CAM6. In addition, the observed north-eastward tilt in the convection band is underestimated in CAM simulations (lower eastward tilt), although with a larger spatial extent.

Further, from the Hovmöller diagram of MISO (Fig. 6), we find that the north-eastward propagation of convection from central EIO to the Indian subcontinent in CAM6 is consistent with observations but shows a weaker eastward component. CAM4 and CAM5 also capture northward propagation, but convection initiates over southern peninsular India instead of central EIO between day -30 to -20. Furthermore, the observed eastward propagating component of MISO is simulated westward in CAM4 and CAM5 (i.e., the north-eastward propagation of convection anomalies is simulated north-westward). This indicates that MISO simulations have improved over time in the subsequent CAM variants, with CAM6 showing the highest improvement.

Further, the important atmospheric processes are analyzed to understand how the MISO has improved in the subsequent CAM variants. Previous research has highlighted the role of atmospheric internal dynamics along with easterly wind shear and meridional asymmetry in specific humidity on the underlying mechanism of MISO (e.g., Webster 1983; Wang and Xie 1997; Jiang et al. 2004, 2011; Abhik et al. 2013). Previous studies have also suggested that improvement in the simulation of seasonal mean climatology from the equator to 15°N, as well as improvement in the movement of convection band from the equator to monsoon trough, are linked to improvements in the simulation of seasonal mean heat source in the EIO region and its interaction with regional and planetary-scale circulations (Attada et al. 2014). Hence, we next analyze the regional Hadley and planetary-scale Walker circulations and the model's internal dynamics in the following subsections.

3.4.1 Hadley and Walker Circulations

The regional Hadley and the planetary-scale Walker circulations are crucial elements of ISM circulation (Oort and Rasmusson 1971; Rao 1976; Sikka 1980; Krishnamurthy and Kinter 2003; Gadgil 2003; Annamalai et al. 2007; Lau et al. 2015; Fan et al. 2017). The movement of the equatorial heat source influences the seasonal mean Walker circulation, while the intensity and position of the monsoon heat source can affect the regional Hadley circulation (e.g., Goswami et al. 1999). Thus, both the atmospheric circulations associated with the heat sources can strongly affect the distribution of seasonal mean precipitation during ISM. From Figure 7 for Hadley circulation, we find the observed subsidence over the southern Indian ocean beyond 10°S and ascent over 10°S to 25°N. CAM3 shows ascending motion over the equator through 25°N (with the strongest ascent over the equator and 12°N), likely associated with higher precipitation over EIO and AS (Fig. 1), leading to weaker northward propagation of equatorial convection to the Indian subcontinent (Sharmila et al. 2013). This stronger than observed ascending motion over the equatorial region seen in CAM3 is improved in CAM4, but the ascent over 12°N is slightly increased with an increased precipitation bias over AS, although a small improvement in northward propagation of convection from the equator is noted from improved ascent over EIO. Subsequent CAM variants (CAM5 and CAM6) show improved simulations of ascent over 12°N, leading to improved northward propagation and spatial pattern of precipitation (Fig. 1). Similar to Hadley circulation, from Figure 8 (Walker circulation), we find observed subsidence over 40°-65°E and ascent over 65°-160°E (Walker 1924; Sikka 1980; Power and Kociuba 2011). In CAM3, the subsidence is largely underestimated (almost absent), and the ascent over 60°E is highly overestimated, likely associated with precipitation

overestimation over WEIO and poor MISO simulation. Subsequent CAM variants improve this overestimation in ascending motion and underestimation in subsidence. Specifically, CAM6 simulates the Walker circulation closer to observation. Thus, we can speculate that the east-west heat source associated with Walker circulation and the monsoon heat source associated with Hadley circulation, which was poorly simulated in CAM3, have improved in subsequent CAM variants.

3.4.2 Atmospheric Internal dynamics

Figure 9 shows the JJAS mean meridional variation of total precipitation, vertical easterly wind shear (U200-U850; m/s), and specific humidity at 1000 hPa, averaged over the longitudinal domain of 70°-90°E for ERA-I and CAM variants. It is noted that the magnitude of total precipitation is greatly overestimated over 10°S and underestimated over Indian latitudes in CAM3 (Fig. 9a). While in subsequent CAM variants, this overestimation in precipitation over 10°S is improved, the underestimation over Indian latitudes is slightly overestimated. Further, from the vertical easterly wind shear, we find that it is highly underestimated in CAM3 from the southern Indian ocean (10°S) to Indian latitudes (up to 20°N), with the highest underestimation over EIO (Fig. 9b). This underestimation is also improved in subsequent CAM variants, with CAM6 showing the highest improvement. Furthermore, the meridional gradient of specific humidity is simulated comparable to ERA-I in all CAM variants, except an overestimation by 2g/kg across the latitudes from 20°S to Indian land (20°N) in CAM3. However, it is noted that the meridional gradient of specific humidity from ocean to land is improved in subsequent CAM variants, with the highest improvement in CAM6, likely an underlying reason for the large improvement in the northward propagation of MISO (e.g., Jiang et al. 2004; Drbohlav and Wang 2005). Improvements in meridional gradient of specific humidity and hence MISO contribute to improvements in JJAS seasonal mean rainfall in successive CAM variants.

Summary And Conclusion

In this study, we have evaluated ISM simulation in four successive versions of the NCAR CAM (CAM3, 4, 5, and 6) to assess the impact of various changes to the model during the last two decades. Improved total precipitation simulation is reported in successive CAM variants, except the wet bias over WGs and Himalayan foothills, which is slightly worsened. This increase in wet bias is due to increasing convective and large-scale precipitation components, respectively. Also, all CAM variants show improvements in the annual precipitation cycle as well as monsoon withdrawal; however, the total precipitation during the monsoon peak period is slightly worsened in the subsequent CAM variants. Further, the aforementioned improvements in ISM rainfall are found to be associated with improvements in TEJ and STJ. In addition, there are improvements in tropospheric temperature gradient and easterly wind shear, resulting in improved northward transport of moisture towards BoB and central India and hence improving the precipitation distribution over the ISM region.

Regarding the intra-seasonal variations of ISM, we have evaluated MISO simulations (initiation of organized convection over central EIO and its north-eastward movement towards the monsoon trough).

We find that CAM3 fails to capture the pattern, but it is improved in subsequent CAM versions. However, the observed north-eastward tilt in the convection band is still largely underestimated in CAM variants. Further, from the northward and eastward component analysis, the improvement in the northward propagating component of MISO is found in the successive CAM variants, but the observed eastward propagating component is still simulated westward. In addition, the analysis of underlying MISO mechanisms has shown that the improvement in MISO in successive CAM variants is likely due to the improvement in the simulation of monsoon and equatorial heat source associated with regional Hadley and planetary-scale Walker circulation. Along with these underlying mechanisms, substantial improvements in the simulation of the atmospheric internal dynamics associated with vertical easterly wind shear and surface specific humidity in subsequent CAM variants could be another reason for the likely improvements in MISO and seasonal mean rainfall.

Overall, the development cycle from CAM3 to CAM4 led to large improvement in most of the ISM features, except the deterioration of the monsoon low level jet. The subsequent development cycles from CAM4 to CAM5 and that from CAM5 to CAM6 showed mixed changes to the quality of simulations with some improvements and some deteriorations in ISM features. For example, in CAM6 the ISM mean total and convective precipitation and MISO, along with the associated circulation features including the regional Hadley circulation, planetary scale Walker circulation, and TEJ were better simulated than all the previous versions of CAM. However, ISM features such as the monsoon onset and the low level jet kept deteriorating in successive development cycles, with CAM6 performing worse than all the previous versions. A summary of the relative performance of the model variants for the various ISM features is presented in Table 2. Finally, some important biases (e.g., eastward component of MISO, monsoon low-level jet, excessive precipitation over Himalayan foothills, early monsoon onset, underestimated extreme and overestimated low precipitation rates) still persist, and need to be alleviated in future versions of CAM.

Declarations

Acknowledgments:

The authors wish to acknowledge NCAR’s climate modeling section (http://www.cgd.ucar.edu/) for developing CAM3, CAM4, CAM5, and CAM6 models. We are thankful to TRMM (https://pmm.nasa.gov/trmm) and ECMWF (https://www.ecmwf.int/en/forecasts/datasets/) for providing the necessary observational and reanalysis datasets publicly. The IITD supercomputing facility is used for the computations. NCAR-NCL is used for data analysis, and climate data operator is used for data processing. This work is partly supported by the DST Centre of Excellence in Climate Modeling at IIT Delhi and through a DST Science and Engineering Research Board (SERB) project (ECR/2015/000229).

Competing Interests

The authors declare no competing financial interests

Data Availability

The observed data used in this study is publicly available and the model simulated data can be obtained from the corresponding author.

Funding

This work is partly supported by the DST Centre of Excellence in Climate Modeling at IIT Delhi and through a DST Science and Engineering Research Board (SERB) project (ECR/2015/000229). Ravi Kumar acknowledges the MTech fellowship from MHRD.

Author's Contribution

SS and RP designed the study with a key input from SKM. RK performed the model simulations and worked with RP for analysis. All authors have contributed in writing the manuscript.

Code Availability

The climate model used for simulations are freely available at https://www.cesm.ucar.edu/ and the code used for figure generation is available with corresponding author and can be obtained on request.

Ethics approval

The manuscript is conducted within the ethical manner advised by the *Theoretical and Applied Climatology.*

Consent to participate

Not applicable

Consent for publication

The research is scientifically consent to be published

References

1. Abhik S, Halder M, Mukhopadhyay P, Jiang X, Goswami BN (2013) A possible new mechanism for northward propagation of boreal summer intra-seasonal oscillations based on TRMM and MERRA reanalysis. Clim Dyn 40:1611–1624
2. Anand A et al (2018) Indian Summer Monsoon Simulations: Usefulness of Increasing Horizontal Resolution, Manual Tuning, and Semi-Automatic Tuning in Reducing Present-Day Model Biases. Sci Rep 8:3522. https://doi.org/10.1038/s41598-018-21865-1
3. Annamalai H, Hamilton K, Sperber KR (2007) The South Asian Summer Monsoon and Its Relationship with ENSO in the IPCC AR4 Simulations. J Clim 20:1071–1092.

https://doi.org/10.1175/JCLI4035

4. Annamalai H, Slingo JM (2001) Active/break cycles: diagnosis of the intra-seasonal variability of the Asian summer monsoon. Clim Dyn 18:85–102
5. Attada R, Parekh A, Chowdary J, Gnanaseelan C (2014) Assessment of the Indian summer monsoon in the WRF regional climate model. Clim Dyn 44:3077–3100. https://doi.org/10.1007/s00382-014-2295-1
6. Bogenschutz PA, Gettelman A, Morrison H, Larson VE, Craig C, Schanen DP (2013) Higher-order turbulence closure and its impact on climate simulations in the community atmosphere model. J Clim 26(23):9655–9676
7. Bollasina M, Nigam S (2009) Indian Ocean SST, evaporation, and precipitation during the South Asian summer monsoon in IPCC-AR4 coupled simulations. Clim Dyn 33:1017–1032. https://doi.org/10.1007/s00382-008-0477-4
8. Collin WD, Rasch PJ, Boville BA, Hack JJ, McCaa JR, Williamson DL, Kiehl JT, Briegleb B, Bitz C, Lin SJ, Zhang M, Dai Y (2004) Description of the NCAR Community Atmosphere Model (CAM3). Technical Report NCAR/TN-464 + STR, National Center for Atmospheric Research, Boulder, Colorado 80307 – 3000, 226 pp
9. Covey C, AchutaRao KM, Cubasch U, Jones P, Lambert SJ, Mann ME, Phillips TJ, Taylor KE (2003) An overview of results from the coupled model intercomparison project (CMIP). Glob Plan Chang 37:103–133. http://dx.doi.org/10.1016/S0921-8181(02)00193-5
10. Dai A (2006) Precipitation characteristics in eighteen coupled climate models. J Climatol 19:4605–4630. https://doi.org/10.1175/JCLI3884.1
11. Dee et al (2011) The ERA-Interim reanalysis: Configuration and performance of the data assimilation system. Quart J Roy Meteor Soc 137:553–597. https://doi.org/10.1002/qj.828
12. Deng ZY, Zhang Q, Yin XZ, Zhang CJ, Xin JW, Liu DX, Pu JY, Dong AX (2007) Drought disaster response to drought climate change. Glac Froz Soil 1:114–118
13. Dey B (1970) Rainfall variability during the Indian summer monsoon. M.S. thesis, Dept. of Geography, University of Wisconsin, 129 pp
14. Douville H, Royer JF, Polcher J, Cox P, Gedney N, Stephenson D, Valdes P (2000) Impact of CO_2 Doubling on the Asian Summer Monsoon: Robust Versus Model-dependent Responses. J Meteoro Soc of Japan. https://doi.org/10.2151/jmsj1965.78.4_421
15. Drbohlav HKL, Wang B (2005) Mechanism of the northward propagating Intra-seasonal oscillations: insight from a zonally symmetric model. J Clim 18:952–972
16. Dunning CM, Turner AG, Brayshaw DJ (2015) The impact of monsoon intra-seasonal variability on renewable power generation in India. Environ Res Lett 10:064002. https://doi.org/10.1088/1748-9326/10/6/064002
17. Fasullo J, Webster PJ (2003) A Hydrological Definition of Indian Monsoon Onset and Withdrawal. Journal of Climate 16.19: 3200–3211. https://doi.org/10.1175/1520-0442(2003)016<3200a:AHDOIM>2.0.CO;2.

18. Fan F, Dong X, Fang X, Xue F, Zheng F, Zhu J (2017) Revisiting the relationship between the South Asian summer monsoon drought and El Niño warming pattern. Atmos Sci Lett 18:175–182. https://doi.org/10.1002/asl.740
19. Indian Meteorological Department (1972) Upper Air Atlas of India and Neighborhood.IMD, New Delhi,60 pp
20. Gadgil S (2003) The Indian monsoon and its variability. Annual Review of Earth Plane Sci 31:429–467. https://doi.org/10.1146/annurev.earth.31.100901.141251
21. Gadgil S, Gadgil S (2006) The Indian Monsoon, GDP and Agriculture. Econo Polit Weekly 41:4887–4895
22. Gadgil S, Sajani S (1998) Monsoon precipitation in the AMIP runs. Clim Dyn 14:659–6889. https://doi.org/10.1007/s003820050248
23. Gent PR, Yeager S, Neale RB, Levis S, Bailey D (2009) Improvements in a half degree atmopshere/land version of the CCSM. Clim Dyn 79:25–58
24. Gettelman A, Morrison H (2015) Advanced two-moment bulk microphysics for global models. part i: off-line tests and comparison with other schemes. J Clim 28(3):1268–1287
25. Gill AE (1980) Some simple solutions for heat-induced tropical circulation. Quart J Roy Meteor Soc 106:447–462. https://doi.org/10.1002/qj.49710644905
26. Golaz JC, Larson VE, Cotton WR (2002) A pdf-based model for boundary layer clouds. part i: method and model description. Journal of the atmospheric sciences 59(24):3540–3551
27. Goswami BN, Annamalai H, Krishnamurthy V (1999) A broad scale circulation index for inter-annual variability of the Indian summer monsoon. Quart J Roy Meteor Soc 125:611–633. https://doi.org/10.1002/qj.49712555412
28. Goswami BN (1998) Interannual variation of Indian summer monsoon in a GCM: external conditions versus internal feedbacks. J Clim 11:501–522
29. Goswami BN, Xavier PK (2005) ENSO control on the South Asian monsoon through the length of the rainy season. Geo-physical Research Letters 32:L18717. https://doi.org/10.1029/2005GL023216
30. Goswami BN (2011) South Asian summer monsoon. In: Lau WK-M, Waliser DE (eds) Intra-seasonal variability of the atmosphere-Ocean climate system, 2nd edn. Springer, Berlin, pp 21–72
31. Huffman GJ et al (2007) The TRMM multi-satellite precipitation analysis: quasi-global, multi-year, combined-sensor precipitation estimates at fine scale. J Hydrometeorol 8:33–55
32. Jiang X, Li T, Wang B (2004) Structures and mechanisms of the northward propagating boreal summer intra-seasonal oscillation. J Clim 17:1022–1039
33. Jiang X, Waliser DE, Li JL, Woods C (2011) Vertical cloud structures of the boreal summer intra-seasonal variability based on CloudSat observations and ERA-interim reanalysis. Clim Dyn 36:2219–2232
34. Joseph S, Sahai AK, Goswami BN (2009) Eastward propagating MJO during boreal summer and Indian monsoon droughts. Clim Dyn 32:1139–1153. https://doi:10.1007/s00382-008-0412-8

35. Joseph et al (2012) Possible role of warm SST bias in the simulation of boreal summer monsoon in SINTEX-F2 coupled model. Clim Dyn 38:1561–1576. https://doi:10.1007/s00382-011-1264-1
36. Kanamitsu M, Krishnamurti TN, Depradine C (1972) On scale interactions in the Tropics during northern summer. J Atmos Sci 29:698–706
37. Knutti R, Masson D, Gettelman A (2013) Climate model genealogy: Generation CMIP5 and how we got there. Geophys Res Lett 40:1194–1199. https://doi.org/10.1002/grl.50256
38. Kobayashi N (1974) Interannual variations of tropical easterly jet stream and rainfall in South Asia. Geophys Mag 37:123–134
39. Koteswaram P (1958) The easterly jet stream in the tropics. Tellus 10(1):43–57. https://doi.org/10.1111/j.2153-3490.1958.tb01984.x
40. Koul V, Parekh A, Srinivas G, Kakatkar R, Chowdary JS, Gnanaseelan C (2018) Role of ocean initial conditions to diminish dry bias in the seasonal prediction of Indian summer monsoon rainfall: A case study using climate forecast system. J Adva Model Earth Sys 10:603–616. https://doi.org/10.1002/2017MS001129
41. Krishnamurthy V, Kinter JL-II (2003) The Indian monsoon and its relation to global climate variability. In: Global Climate Berlin. Springer, Heidelberg, pp 186–236
42. Krishnan R, Kumar V, Sugi M, Yoshimura J (2009) Internal feedbacks from monsoon–midlatitude interactions during droughts in the Indian summer monsoon. J Atmos Sci 66:553–578
43. Kumar B, Naidu C, Rao S (2004) Influence of southern oscillation and SSTs over Niño-3.4 region on the winter monsoon rainfall over coastal Andhra Pradesh. J Earth Sys Sci 113:313–319. https://doi.org/10.1007/bf02716728
44. Lau KM, Yang S (2015) Tropical Meteorology and Climate | Walker Circulation. Encyclo Atmos Sci. https://doi.org/10.1016/B978-0-12-382225-3.00450-3
45. Mishra SK, Anand A, Fasullo J, Bhagat S (2018) Importance of the resolution of surface topography in indian monsoon simulation. J Clim 31:4879–4898. https://doi.org/10.1175/JCLI-D-17-0324.1
46. Neale RB, Richter JH, Jochum M (2008) The impact of convection on ENSO: From a delayed oscillator to a series of events. J Clim 21:5904–5924. http://dx.doi.org/10.1175/2008JCLI2244.1
47. Neale RB et al (2010) Description of the NCAR Community Atmosphere Model (CAM 4.0).NCAR Tech Note NCARTN- 485 + STR, Boulder, Colorado, USA. pp. 212
48. Neale RB et al (2012) Description of the NCAR Community Atmosphere Model (CAM 5.0).NCAR Tech Note NCARTN- 486 + STR, Boulder, Colorado, USA. pp. 274
49. Oort AH, Rasmusson EM (1971) Atmospheric Circulation Statistics. NOAA Prof. Pap. No. 5. U.S. Government Printing Office
50. Pathak R, Sahany S, Mishra SK, Dash SK (2019) Precipitation biases in CMIP5 models over the south Asian region. Sci Rep 9:9589. https://doi.org/10.1038/s41598-019-45907-4
51. Pathak R, Sahany S, Mishra SK (2020) Uncertainty quantification based cloud parameterization sensitivity analysis in the NCAR community atmosphere model. Sci Rep 10:17499.

https://doi.org/10.1038/s41598-020-74441-x

52. Parthasarathy BA, Munot AA, Kothawale DR (1988) Regression model for estimation of foodgrain production from summer monsoon rainfall. Agricultural Forest Meteoro 42:167–182. https://doi.org/10.1016/0168-1923(88)90075-5
53. Park S, Bretherton CS (2009) The University of Washington shallow convection and moist turbulence schemes and their impact on climate simulations with the Community Atmosphere Model. J Clim 22:3449–3469. https://doi.org/10.1175/2008JCLI2557.1
54. Park S, Bretherton CS, Rasch PJ (2010) The revised cloud macrophysics in the community atmosphere model. J Clim
55. Pascale S, Lucarini V, Feng X, Porporato A, Hasson S (2014) Analysis of rainfall seasonality from observations and climate models. Clim Dyn. https://doi.org/10.1007/s00382-014-2278-2
56. Pielke et al (2001) Analysis of 200 mbar zonal wind for the period 1958–1997. J Geophys Res 106:27,287–227,290. https://doi.org/10.1029/2000JD000299
57. Power SB, Kociuba G (2011) The impact of global warming on the Southern Oscillation Index. Clim Dyn 37(9–10):1745–1754. https://doi.org/10.1007/s00382-010-0951-7
58. Rajeevan M, Unnikrishnan C, Bhate J, Niranjan KK, Sreekala P (2012) Northeast monsoon over India: variability and prediction. Meteor App 19:226– 236. https://doi.org/10.1002/met.1322
59. Ramaswamy C (1962) Breaks in the Indian summer monsoon as a phenomenon of interaction between the easterly and the sub-tropical westerly jet streams. Tellus 14, 337– 349. https://doi.org/10.1111/j.2153-3490.1962.tb01346.x
60. Ramu DA, Sabeerali CT, Chattopadhyay R, Rao DN, George G, Dhakate AR, Salunke K, Srivastava A, Rao SA (2016) Indian summer monsoon rainfall simulation and prediction skill in the CFSv2 coupled model: Impact of atmospheric horizontal resolution. J Geophys Res: Atmos 121:2205–2221. https://doi.org/10.1002/2015JD024629
61. Rao YP (1976) Southwest monsoon: Synoptic Meteorology, Meteor. Monogr., No. 1/1976. India Meteorological Department, 367 pp
62. Ratna et al (2014) Moisture Trend over the Arabian Sea and Its Influence on the Indian Summer Monsoon Rainfall. CMCC Res. Papers, Issue RP0225
63. Reynolds RW, Rayner NA, Smith TM, Stokes DC, Wang W (2002) An improved in situ and satellite SST analysis for climate. J Clim 15:1609–1625
64. Richter JH, Rasch PJ (2008) Effects of Convective Momentum Transport on the Atmospheric Circulation in the Community Atmosphere Model, Version 3. J Clim 21:1487–1499. https://doi.org/10.1175/2007JCLI1789.1
65. Roxy et al (2012) Intra-seasonal SST-precipitation relationship and its spatial variability over the tropical summer monsoon region. Clim Dyn. https://doi.org/10.1007/s00382-012-1547-1
66. Sahany S, Saroj KM, Pathak R, Rajagoplan B (2018) Spatio-Temporal Variability of Seasonality of Rainfall over India. Geophys Res Lett 45(14):7140–7147. https://doi.org/10.1029/2018GL077932

67. Salunke P, Jain S, Mishra SK (2019) Performance of the CMIP5 models in the simulation of the Himalaya-Tibetan Plateau monsoon. Theor Appl Climatol 137:909–928. https://doi.org/10.1007/s00704-018-2644-9
68. Sathiyamoorthy V (2005) Large scale reduction in the size of the tropical easterly jet. Geophys Res Lett 32:L14802. https://doi.org/10.1029/2005GL022956
69. Sikka DR (1980) Some aspects of the large scale fluctuations of summer monsoon rainfall over India in relation to fluctuations in the planetary and regional scale circulation parameters. J Earth Syst Sci 89:179–195. https://doi.org/10.1007/BF02913749
70. Sikka DR, Gadgil S (1980) On the maximum cloud zone and the ITCZ over Indian, longitudes during the southwest monsoon. Mon Weather Rev 108:1840–1853
71. Sharmila S, Pillai PA, Joseph S, Roxy M, Krishna RPM, Chattopadhyay R, Abhilash S, Sahai AK, Goswami BN (2013) Role of ocean–atmosphere interaction on northward propagation of Indian summer monsoon intra-seasonal oscillations (MISO). Clim Dyn 41:1651–1669. https://doi.org/10.1007/s00382-013-1854-1
72. Sperber et al (2013) The Asian summer monsoon: An intercomparison of CMIP5 vs. CMIP3 simulations of the late 20th century. Clim Dyn 41:2711– 2744. https://doi.org/10.1007/s00382-012-1607-6
73. Sreekala et al (2014) A study on the decreasing trend in tropical easterly jet stream (TEJ) and its impact on Indian summer monsoon rainfall.Theor App Climato 118:107–114. https://doi.org/10.1007/s00704-013-1049-z
74. Swapna et al (2002) Role of low level flow on the summer monsoon rainfall over the Indian subcontinent during two contrasting monsoon years. J. Indian Geophys. Uni. 6
75. Sukumaran S, Ajayamohan R (2014) Origin of cold bias over the Arabian Sea in Climate Models. Sci Rep 4. https://doi.org/10.1038/srep06403
76. Trenberth KE, Dai A, Rasmussen RM, Parsons DB (2003) The Changing Character of Precipitation. Bull Amer Meteor Soc 84:1205–1218. https://doi.org/10.1175/BAMS-84-9-1205
77. Vavrus S, Waliser D (2008) An improved parameterization for simulating Arctic cloud amount in the CCSM3 climate model. J Clim 21, 5673–5687. https://doi.org/10/1175/2008JCLI2299.1
78. Walker GT (1924) Correlation in seasonal variations of weather, IX: A further study of world weather. Mem Ind Meteor Dept 24:275–332
79. Wang B, Xie X (1997) A model for the boreal summer intra-seasonal oscillations. J Atmos Sci 54:72–86
80. Webster PJ, Magana VO, Palmer TN, Shukla J, Thomas RA, Yani M, Yasunari T (1998) The monsoon: processes, predictability and prediction. J Geophys Res 103:14451–14510. https://doi.org/10.1029/97JC02719
81. Webster PJ, Yang S (1992) Monsoon and ENSO:Selectively interactive system. Q J R Meteorol Soc 118:877–926

82. Webster PJ (1983) Mechanisms of monsoon low-frequency variability: surface hydrological effects. J Atmos Sci 40:2110–2124
83. Xavier PK, Marzin C, Goswami BN (2007) An objective definition of the Indian summer monsoon season and a new perspective on the ENSO–monsoon relationship. Q J R Meteorol Soc 133:749–764
84. Yanai M, Esbensen S, Chu J (1973) Determination of the bulk properties of tropical cloud clusters from large heat and moisture budgets. J Atmos Sci **30**, 611–627. https://doi.org/10.1175/1520-0469(1973)030<0611:DOBPOT>2.0.CO;2.
85. Zhou L, Murtugudde R (2014) Impact of northward-propagating intra-seasonal variability on the onset of Indian summer monsoon. J Clim 27:126–139
86. Zhou ZQ, Xi SP, Zheng XT, Liu Q, Wang H (2014) Global warming–induced changes in El Niño teleconnections over the North Pacific and North America. J Clim 27(24):9050–9064

Tables

Table 1. List of parameterization schemes used in CAM variants

Scheme	CAM3	CAM4	CAM5	CAM6
Deep Convection	*Zhang and McFarlane (1995)*	*Neale et al. (2008)*	*ZM, Neale et al. (2008)*	*ZM, Neale et al. (2008,2017)*
Shallow Convection	*Hack (1994)*	*Richter and Rasch (2008)*	*Park et al. (2009)*	*CLUBB: Boggenschutz et al. (2013)*
Microphysics	*Rasch and Kristjansson (1998)*	*Rasch and Kristjansson (1998)*	*Morrison and Gettelman (2008)*	*Gettelman-Morrison (2015)*
Macrophysics	*Rasch and Kristjansson (1998)*	*Rasch and Kristjansson (1998)*	*Park et al. (2011)*	*CLUBB: Boggenschutz et al. (2013)*
PBL scheme	*Holtslag and Boville (1993)*	*Holtslag and Boville (1993)*	*Bretherton et al. (2009)*	*CLUBB: Boggenschutz et al. (2013)*
Radiation	*Collins et al. (2001)*	*Collins et al. (2001)*	*Iacono et al. (2008)*	*Iacono et al. (2008)*
Aerosols	*Bulk Aerosol Model*	*Bulk Aerosol Model*	*3-MODE Modal Aerosol Model* *Ghan et al. (2011)*	*4-MODE Modal Aerosol Model Ghan et al. (2011)*

Table 2. Evaluation of ISM simulations in CAM variants in comparison to their predecessor versions (i.e., the performance of CAM4 with respect to CAM3, the performance of CAM5 with respect to CAM3 and

CAM4, and the performance of CAM6 with respect to CAM3, CAM4, and CAM5). The upward arrow highlighted in green represents improvement, while the downward arrow highlighted in red represents deterioration, and the dash represents no significant improvement or deterioration.

	CAM4	CAM5	CAM6
Total Precipitation	↑	↑↑	↑↑↑
Convective precipitation	↑	↑↓	↑↑↑
Large-scale precipitation	↑	↓↓	↑↓↑
Annual cycle	↑	↑↑	↑↑↓
Monsoon onset	↑	↑-	↓↓↓
Monsoon withdrawal	↑	-↓	↑-↑
Extreme precipitation	↑	↑-	↑↓↓
Low-level Jet	↓	↓↑	↓↓↓
Tropical easterly Jet	↑	↑↑	↑↑↑
Monsoon Intra-seasonal Oscillation	↑	↑↓	↑↑↑
Hadley circulation	↑	↑↑	↑↑↑
Walker circulation	↑	↑↓	↑↑↑

Figures

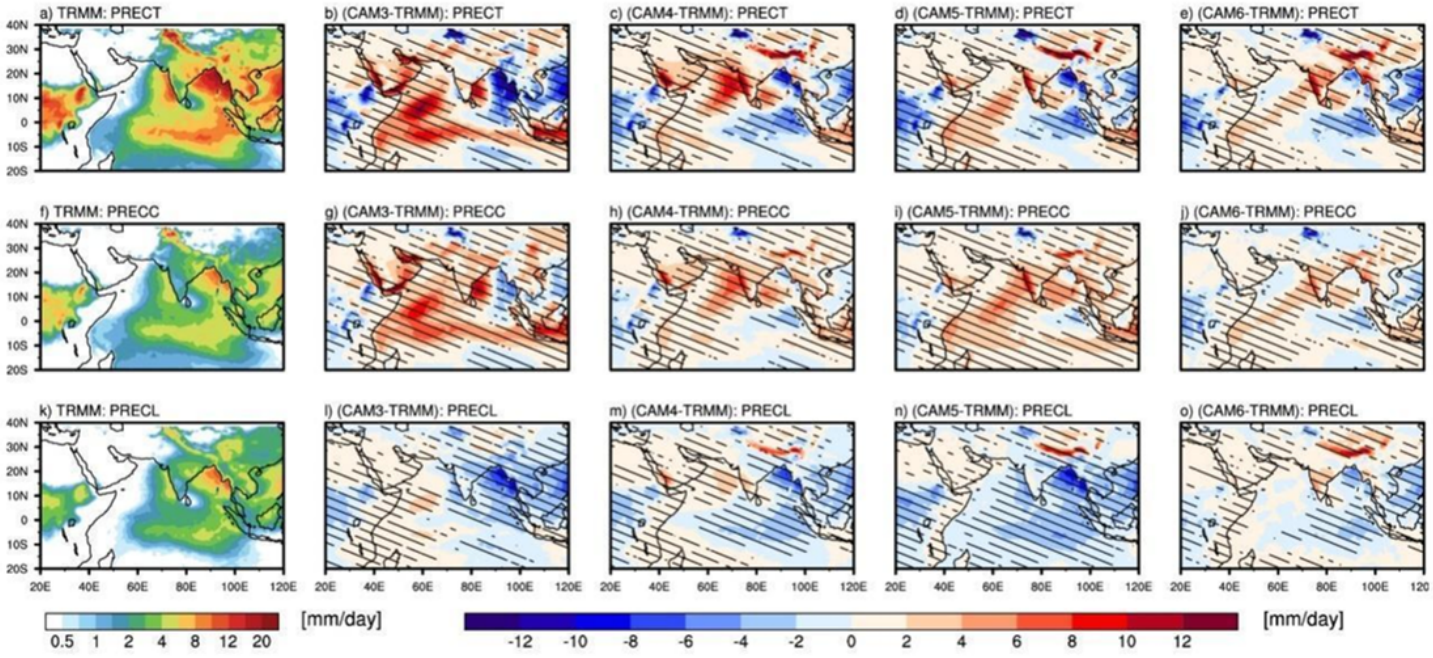

Figure 1

Spatial variation of JJAS mean total precipitation from a) observation (TRMM 3A12), as well as the difference in total precipitation for b) CAM3, c) CAM4, d) CAM5, and e) CAM6, with respect to observation. The spatial pattern of JJAS mean convective precipitation (f-j) and large-scale precipitation

(k-o) is shown in the second and third rows, similarly to total precipitation. The hatched lines in the difference plot show the difference significant at 95 percent confidence level based on the two-tailed Student-t test.

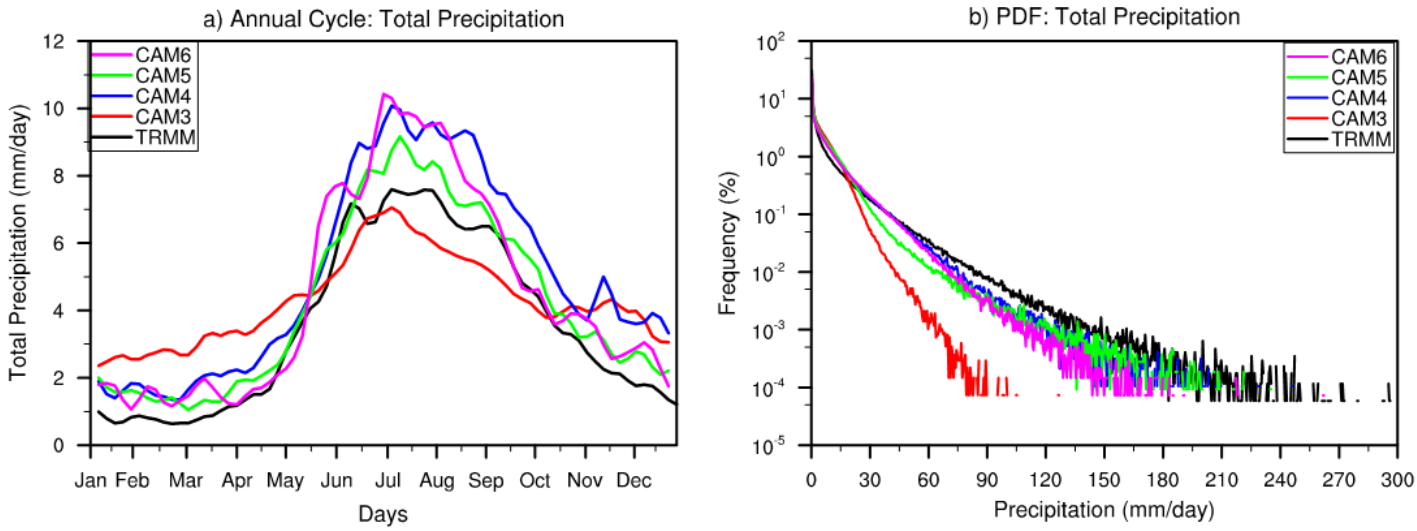

Figure 2

a) Annual cycle of area-averaged total precipitation distribution over the Indian land and b) Probability-intensity distribution of total precipitation over the Indian land during JJAS for observation and different CAM variants.

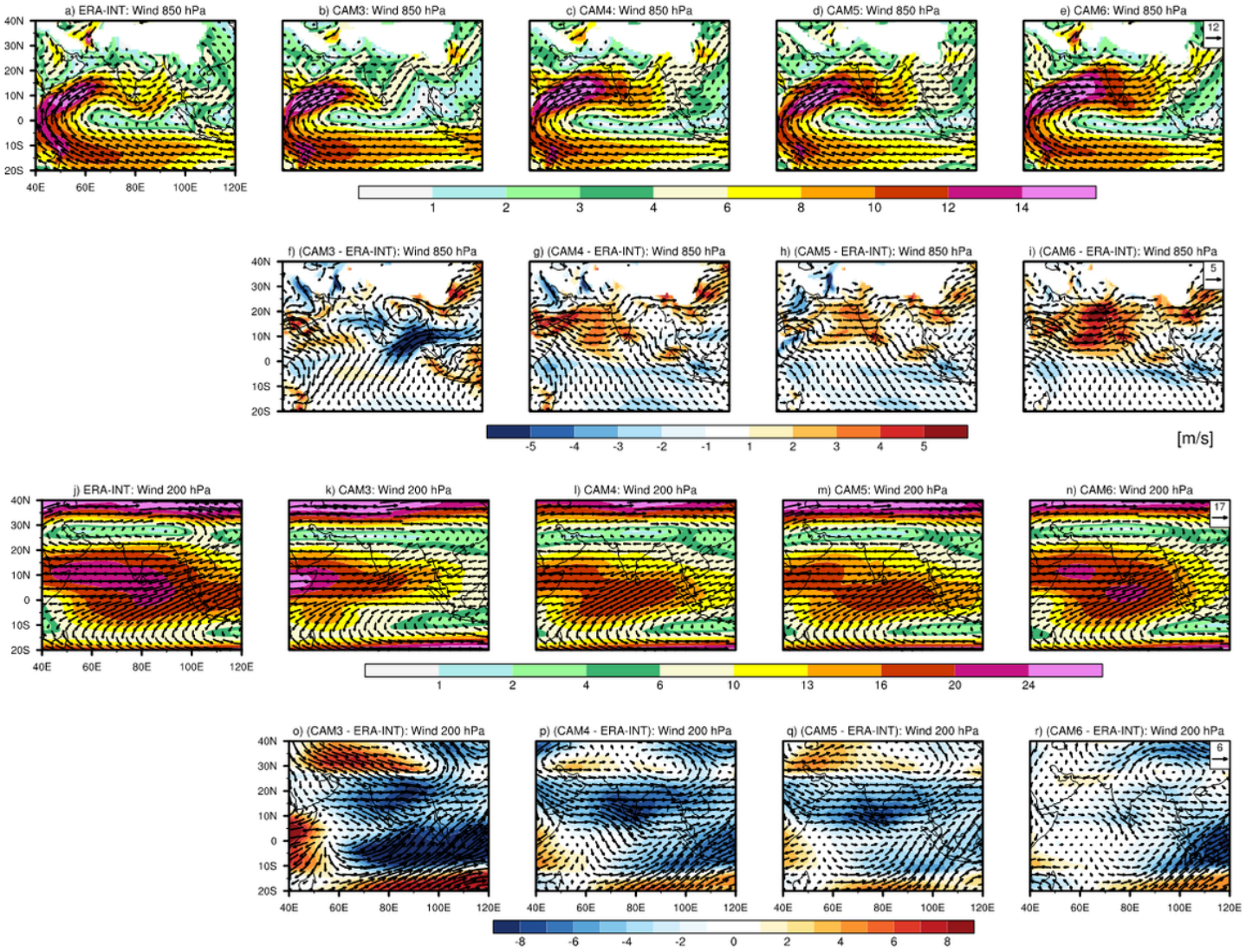

Figure 3

Spatial variation of JJAS mean wind (speed and vectors) at 850 hPa from ERA-I (a) and CAM variants (b-e), and the corresponding difference plot for CAM variants (f-i) with respect to ERA-I. The spatial variation of JJAS mean wind at 200 hPa from ERA-I (j) and CAM variants (k-n), and the corresponding difference plot for CAM variants (o-r) with respect to ERA-I are shown in third and fourth rows, respectively.

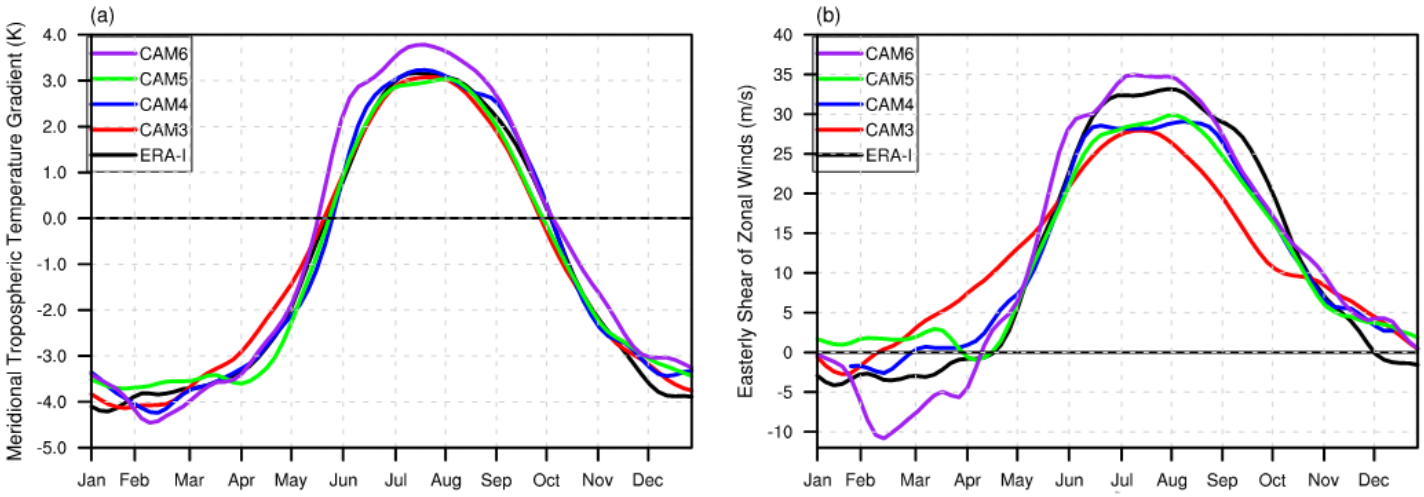

Figure 4

a) Annual cycle of meridional tropospheric temperature gradient (MTTG) and b) annual cycle of easterly shear of zonal wind (ESZW). The vertically averaged (600-200 hPa) temperature difference between the two regions, one over (5N-35N; 40E-100E) and other over (15S-5N; 40E-100E), is used to compute MTTG. The difference between 850 hPa and 200 hPa averaged zonal wind over 0-15N and 50E-90E, is used to compute ESZW.

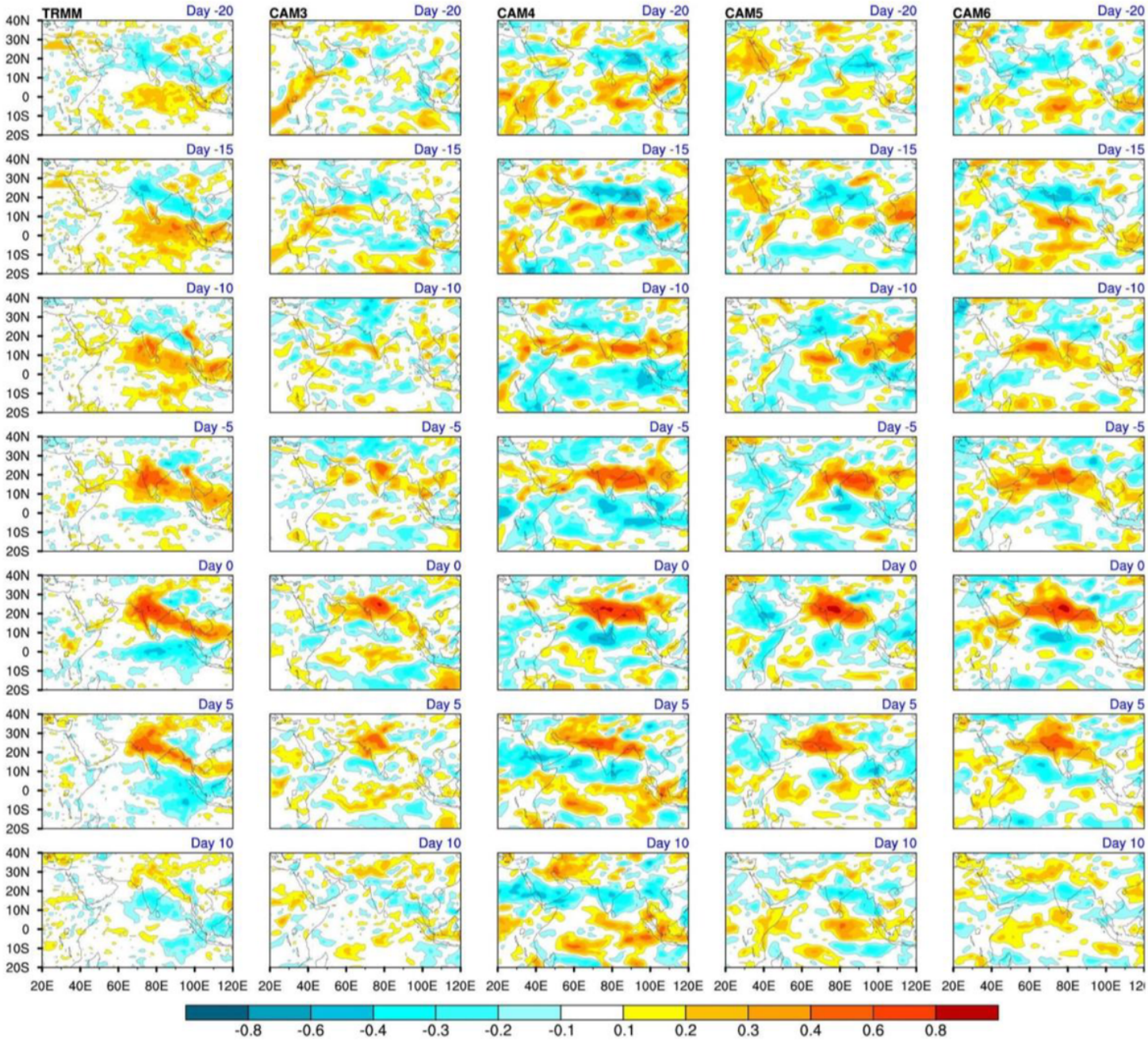

Figure 5

Propagation of the monsoon intra-seasonal oscillation (MISO) from day -20 to day +10 from TRMM and CAM variants. MISO is obtained by regressing the 20-100 day filtered time-series of area-averaged precipitation anomalies over central India (18N-28N; 73E-82E), with the 20-100 day filtered spatial precipitation anomalies.

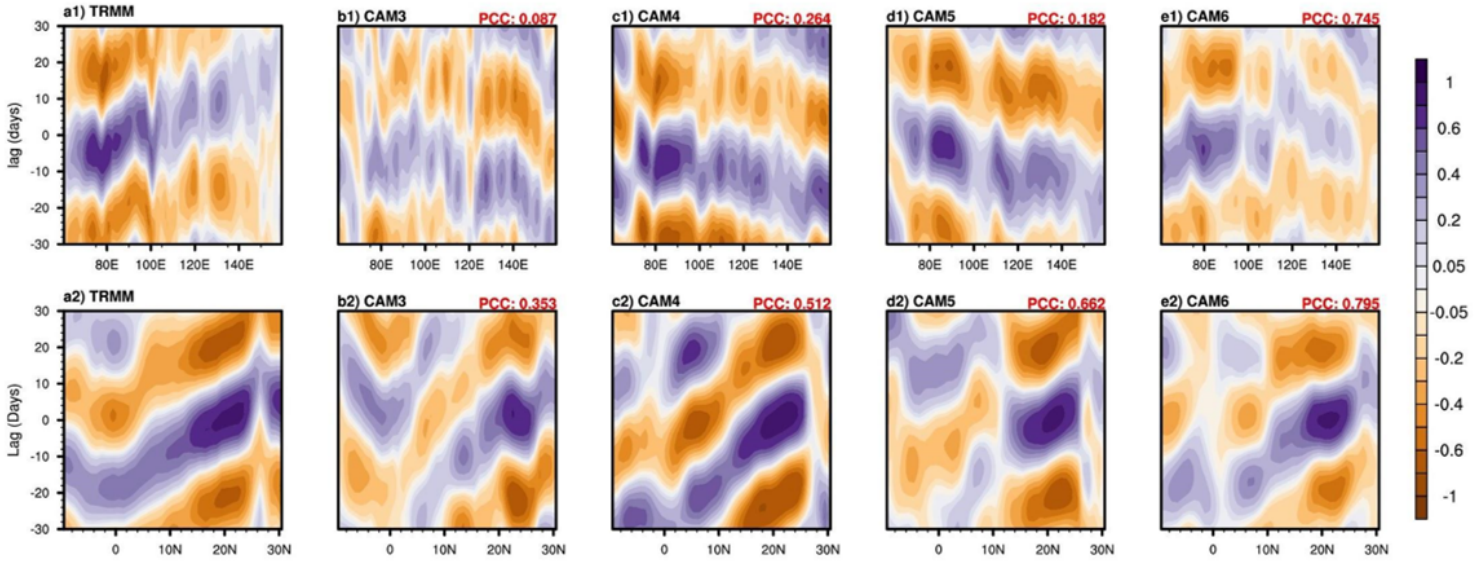

Figure 6

Hovmöller plots of 30-60 day filtered precipitation anomalies regressed with respect to the reference time series averaged over central India for TRMM and CAM variants. The first row shows eastward propagation (averaged over 10N-20N), while the second row shows northward propagation (averaged over 70E-90E).

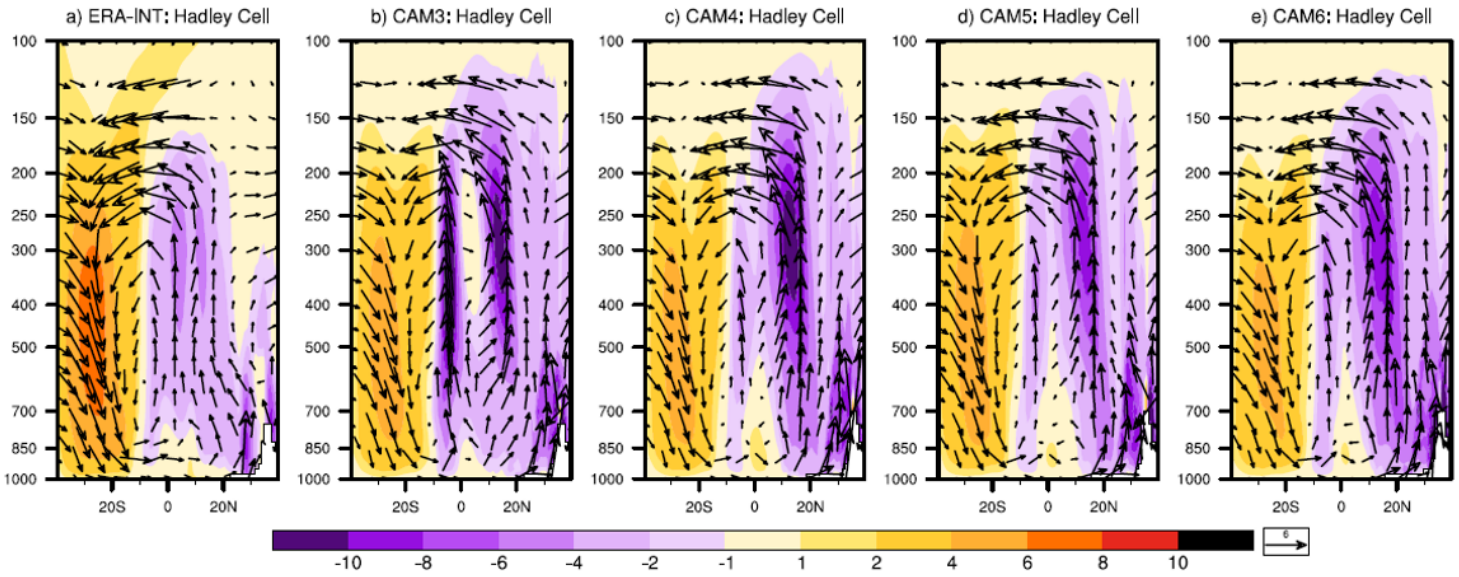

Figure 7

JJAS mean regional Hadley circulation (averaged over 70E-90E) for TRMM, b) CAM3, c) CAM4, d) CAM5, e) CAM6. The vertical wind is multiplied by 100.

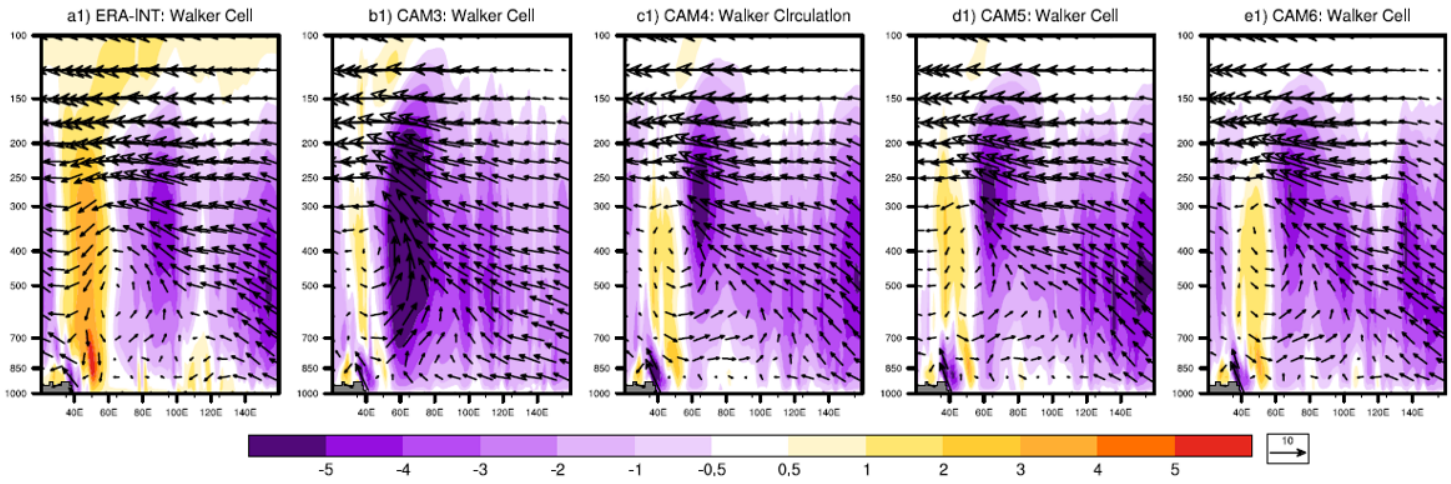

Figure 8

JJAS mean planetary-scale Walker circulation (averaged over 10S-10N) for a) ERA-I, b) CAM3, c) CAM4, d) CAM5, e) CAM6. The vertical wind is multiplied by 100.

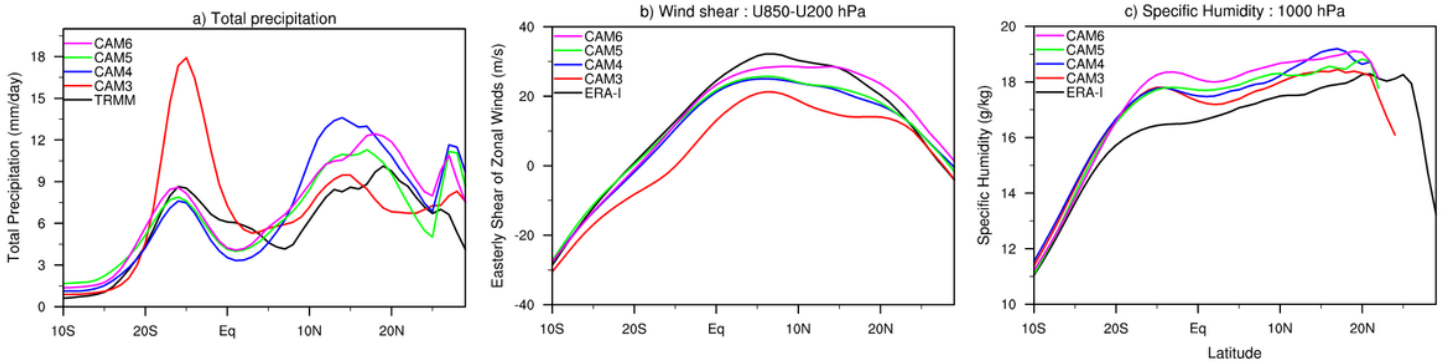

Figure 9

JJAS mean meridional distribution (averaged over 70-90E) of a) total precipitation, b) zonal wind shear (U200 - U850), c) specific humidity from observations/ERA-I and CAM variants.